The Thesis Committee for Youngkyu Lee
Certifies that this is the approved version of the following thesis:

Designs of efficient plasmonic probe for near-field scanning optical microscopy

APPROVED BY
SUPERVISING COMMITTEE:

Supervisor: Andrea Alù

Xiaojing Zhang

Designs of efficient plasmonic probe for near-field scanning optical microscopy

by

Youngkyu Lee, B.S.

Thesis

Presented to the Faculty of the Graduate School of

The University of Texas at Austin

in Partial Fulfillment

of the Requirements

for the Degree of

Master of Science in Engineering

The University of Texas at Austin

May 2012

Abstract

Designs and fabrication of efficient plasmonic probe for near-field scanning optical microscopy

Youngkyu Lee, M.S.E

The University of Texas at Austin, 2012

Supervisor: Andrea Alù and Xiaojing Zhang

We present a novel concept to design apertureless plasmonic probes for near-field scanning optical microscopy (NSOM) with enhanced optical power throughput and near-field confinement. Specifically, we combine unidirectional surface plasmon polariton (SPP) generation along the tip lateral walls with nanofocusing of SPPs through adiabatic propagation towards an apertureless tip. Three probe designs are introduced with different light coupling mechanisms. Optimal design parameters are obtained with 2D analysis and realistic probe geometries with patterned plasmonic surfaces are proposed using the optimized designs. The electromagnetic properties of the designed probes are characterized in the near-field and compared to those of a conventional single-aperture probe with same pyramidal shape. The optimized probes feature enhanced light localization in near-field of tip apex and improved optical throughput. Our ideas effectively combine the resolution of apertureless probes with throughput levels much larger than those available even in aperture-based devices.

Table of Contents

List of Figures

Chapter 1: Introduction

1.1 MOTIVATION

The recent prominent progress in nano-photonics has been made utilizing the properties of localized electromagnetic (EM) waves [1] that are coupled at the metal and dielectric interfaces. Surface plasmons, which follow the evanescent modes of propagation, have enabled distinguishable optical phenomena that never witnessed in the conventional optics and led to the development of important applications such as nanoantenna [1-4], nano grating coupler [5-7], and plasmonic near-field scanning optical microscopy (NSOM) [6,8]. By exploiting the highly confined near-field properties, it has been proven that the efficient optical devices [5, 7-12] featuring low physical profile can be realized. Important optical feature associated with the surface plasmons is the near-field waveguiding and focusing by following the guidance of the bounded oscillatory electrons [1,6]. Within the scope of the capability supported by plasmonic geometry, such as the extraordinary effects achieved with metallic waveguides [12-17], one may extend the use of surface plasmons in any fields which take advantage of efficient controls of photons.

In this thesis, our focus primary centers about the development of efficient plasmonic applications, specifically a plasmonic scanning probe for the near-field scanning optical microscopy In this field of research, the use of surface plasmon encompasses the needs of efficient light concentration and localization mechanisms, which can be easily synthesized and realized within the current nanofabrication capability [18,19], while breaking the limit of conventional microscopy. Presented work includes the process of developing an efficient plasmonic probe starting from the theoretical analysis to the device fabrication. Through the numerical simulations and analytical investigations, we discuss and verify the performance of novel probe designs providing

highly confined electromagnetic energy within small volume of interest. Along with the theoretical studies on proposed probe, we also discuss potential way to realizing the efficient scanning probe within the scope of current MEMS and nanofabrication technologies while providing preliminary fabrication results of probes.

1.2 DIELECTRIC FUNCTION OF MATERIALS

The optical response of material to incident light can be expressed as a complex dielectric function, which is determined by electric and magnetic dipolar moment of oscillating electrons in the target material. Such light-matter interaction in general varies with the condition of exterior electromagnetic excitation introduced around. Although this dielectric function is frequently referred as the optical constant or dielectric constant; however, its value is indeed not constant and shows dispersion over the varying wavelength of operation. In this respect, it is important to properly model the complex dielectric function in regards to performing either theoretical investigation or proper use of surface plasmons which is highly sensitive to the surrounding dielectric function.

For some materials having a nearly permanent dipolar moment operating within the frequency range of interest, such as an air, the dielectric function follows typical constant value for the operation. In contrast, the dielectric properties of novel materials, frequently used as plasmonic materials having high density of electrons, in general follow the frequency dispersion [20,21]. Upon the present moment, several classical, physical models have been introduced to describe the optical properties of plasmonic materials, being based on the mechanical interpretation of the electron movement: Lorentz model, Lorentz-Drude model, extended Drude model, and Debye model. Among them one important modeling methodology of the complex dielectric function, especially in

plasmonics nanophotonics, would be the Lorentz-Drude model treating charge carrier (electron) as damped harmonic oscillators.

$$\varepsilon_{Drude}(\omega) = 1 - \frac{{\omega_p}^2}{\omega^2 + i\Gamma\omega}, \tag{1.1}$$

where ω is the frequency of operation; Γ is the damping frequency; and ω_p the oscillator frequency. The Equation 1.1, Drude model, has well described the dispersion of metals such as Aluminum (Al) and alkali metals in which the major carriers behave similar to free electrons. However, more sophisticated model may be required when the effect of bounded electrons becomes significant. To address the movement of both free electrons and non-negligible bounded electrons, one may use extended Drude model described in the Equation 1.2.

$$\varepsilon_{E.Drude}(\omega) = \varepsilon_{\infty} - \frac{(\varepsilon_{\infty} - \varepsilon_{St}){\omega_p}^2}{\omega^2 + i\Gamma\omega}, \tag{1.2}$$

where ε_{∞} and ε_{St} are the dielectric permittivity at high frequency and low (static) frequency, respectively. Throughout this thesis, the extended Drude model has been employed to explain the dispersion of plasmonic metal, especially silver (Ag) and theoretically characterize the performance of plasmonic device proposed.

1.3 SURFACE PLASMONS AND DISPERSIONS

Surface plasmons are the collective movement of surface charges bounded on a highly conductive surface, performing coherent oscillations and fluctuations. With a harmonized movement, surface plasmons can either stimulate or be excited by the electromagnetic wave, well-defined with Maxwell's equation. In this section, we review

the general properties of surface plasmons and their frequency dispersions with specific boundary conditions. From the given boundary condition, the dispersion can be derived and obtained with Maxwell's equation. To clarify the physical notation of time convention, we note that the factor $\exp(i\omega t)$ is used throughout this thesis to express the time- and phase-evolution of electromagnetic waves.

1.3.1 Surface plasmon on thick metal film

One useful configuration of interest where surface plasmon polaritons (SPPs) can be launched at would be a single interface conjoined with two spectrally-thick dielectric and metal (see Figure 1-1) layer.

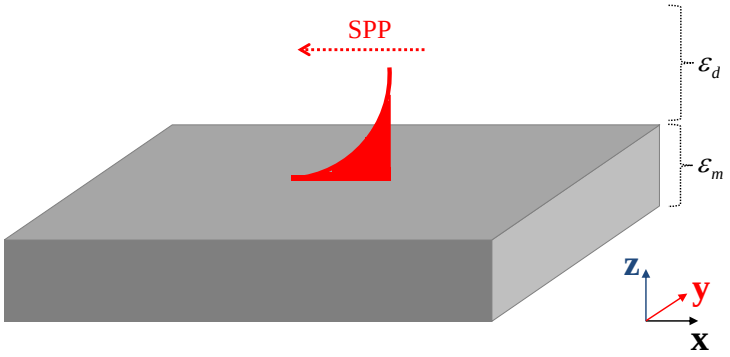

Figure 1-1. Surface plasmon polarition, excited at the interface between spectrally-thick metal film and semi-infinitely thick dielectric medium. Note that ε_m and ε_d are the complex dielectric function of metal and upper medium, respectively.

Since the launched SPPs at the interface decay exponentially along the transverse direction (z-direction) to that of wave propagation, the most of electromagnetic energy is confined in proximity to the interface and easily affected by changes in dielectric properties of surroundings. With such squeezed field distribution, one may tailor surface

plasmons by presenting surface corrugations and abnormalities to out-couple the part of surface optical energy. More details of tailoring surface plasmons are presented in the Section 2.

The dispersion of SPP, the wave in strict transverse magnetic mode (TM), in the given configuration (see Figure 1-1) can be described and understood by solving the boundary condition of the Maxwell's equation. The magnetic field distribution of excited SPP with the wavenumber of k_{spp} is given by

$$\begin{aligned} \mathbf{H}_d(x,z) &= \hat{y} H_o \exp[-ik_{spp}x - \alpha_d z)], \qquad z > 0 \\ \mathbf{H}_m(x,z) &= \hat{y} H_o \exp[-ik_{spp}x + \alpha_m z], \qquad z < 0 \end{aligned} \tag{1.3}$$

where $\alpha_d = \left[-\varepsilon_d {k_0}^2 + {k_{spp}}^2\right]^{1/2}$ and $\alpha_d = \left[-\varepsilon_m {k_0}^2 + {k_{spp}}^2\right]^{1/2}$. And the electric field distribution can be directly derived from the Maxwell's equation. From the field distribution, we can deduce the dispersion relation by solving the Equation 1.3 with the Maxwell's equation and obtain the dispersive wavenumber of SPP

$$k_{spp} = \frac{\omega}{c}\left(\frac{\varepsilon_d \varepsilon_m}{\varepsilon_d + \varepsilon_m}\right)^{1/2}. \tag{1.4}$$

It is important to note that there is the only single mode of surface plasmons can exist on thick metal film by following the transverse resonant mode of operation. Due to the high quality factor of transverse resonance and confined field distribution, for lossy metal case, the energy of surface wave decays fast by the ohmic losses as propagating along the interface, in comparison to the typical propagation length of classical optics. For instance, the expected propagation length $L = \left|2\,\mathrm{Re}[ik_{spp}]\right|^{-1}$ of SPP is in general contained about $20 \sim 30\,\mu\mathrm{m}$ in the visible range. In this respect, it is essential to

fabricate devices within a compact physical dimension to allow for utilizing SPP before the most energy dissipates

1.3.2 Surface plasmon in metal-insulator-metal

Metal-insulator-metal (MIM) configuration, for TM mode of plasmons, can serve as a waveguide allowing the optical energy transmission through very thin dielectric layer. Since there is no fundamental limitation of TM wave transmission on the thickness of dielectric layer, in theory, so that optical energy can be coupled into the thin dielectric layer with proper coupling mechanisms. One useful application related to the MIM geometry in Figure 1-2 is a subwavelength-sized slit which is frequently referred in recent studies on nano-photonics [22]. With expected high impedance mismatch at slit opening, it has been used to couple surface plasmons for various applications.

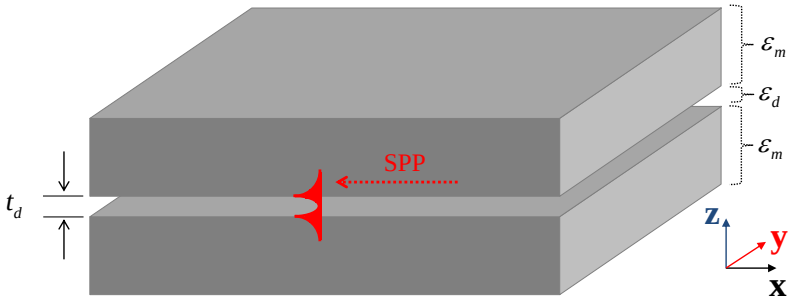

Figure 1-2. Plasmonic waveguidance in MIM structure. Thin dielectric (ε_d) layer is embedded in thick metal (ε_m) layers, with a thickness of t_d.

The TM polarized waves resides inside the dielectric layer may be expressed as a summation of waves, matching with the separate boundary condition of upper and bottom interfaces. With a consideration of traveling wave in x direction with the wave with the

propagating wavenumber of β_x, the magnetic field distribution of the geometry can be expressed as

$$\mathbf{H}(x,z)=\begin{cases}\hat{y}\,H_0\exp[-\alpha_m z]\exp[-i\beta_x x], & (\text{for upper metal layer})\\ \hat{y}\left\{H_1\exp[-i\beta_z z]+H_2\exp[+i\beta_z z]\right\}\exp[-i\beta_x x], & (\text{for dielectric layer})\\ \hat{y}\,H_0\exp[+\alpha_m z]\exp[-i\beta_x x], & (\text{for bottom metal layer})\end{cases} \tag{1.4}$$

where $\alpha_m=\left[\beta_x{}^2-\varepsilon_m k_o{}^2\right]^{1/2}$, $\beta_z=\left|-\beta_x{}^2+\varepsilon_d k_o{}^2\right|^{1/2}$.

Following the boundary conditions at top and bottom interfaces, the supported TM waves would satisfy the dispersion relations:

$$H_1/H_2=\begin{cases}\dfrac{i\beta_z/\varepsilon_d-\alpha_m/\varepsilon_m}{i\beta_z/\varepsilon_d+\alpha_m/\varepsilon_m}\exp[-i\beta_x t_d]\\ \dfrac{i\beta_z/\varepsilon_d+\alpha_m/\varepsilon_m}{i\beta_z/\varepsilon_d-\alpha_m/\varepsilon_m}\exp[i\beta_x t_d]\end{cases} \tag{1.5}$$

The Equation 1.5 implies that there can be multiple waves in TM modes supported by the MIM structure that can be express as the following equation:

$$\exp[in\pi]=\left\{\frac{i\beta_z/\varepsilon_d+\alpha_m/\varepsilon_m}{i\beta_z/\varepsilon_d-\alpha_m/\varepsilon_m}\exp[i\beta_x t_d]\right\}^2,\ \text{for n}\geq 0 \tag{1.6}$$

It has to be noticed that the Equation 1.6 implies significant meaning in the phase evolution of waves, so that more convenient expression may come out with sinusoidal/hyperbolic form as referred in somewhere else [14]. From this analytical solution toward the possible mode calculation inside dielectric film, one can estimate and

determine proper the thickness of dielectric layer for specific wavelength of operation having desired number of TM modes. Moreover, specific values of wavenumber can be extracted out of this equation, determining the characteristic impedance of such MIM geometry.

1.4 SCOPE OF THESIS

The work focused in this thesis falls into the ultimate goal of developing efficient plasmonic scanning probe for NSOM application. To realize the efficient NSOM probe breaking the limit of conventional optics pose, first, theoretical investigations on the plasmonic probe have been carried out with specific emphasis on the efficient use of incident optical energy. Starting from designing and characterizing slit-based surface plasmon coupler that can translate the impinging light into surface waves in unidirectional manner, the idea of efficient control of photons is integrated with the focusing mechanisms of surface waves into the small volume of interest. Various coupling mechanisms have been investigated and synthesized with the metallic scanning probe, and the designed probes are characterized in near-field with full-wave numerical simulations. Before heading toward our ultimate goal to verify and experimentally demonstrate the performance of designed efficient plasmonic scanning probes, we manufacture and realize such probes within the scope of current fabrication capabilities. Silicon based MEMS technologies have been employed along with nano-fabrication technologies, yielding high precision of fabrication.

Our remaining objectives will be the development of overall NSOM system suitable for the designed probes. Upon the development of efficient plasmonic scanning probes and the NSOM system that we have dedicated on, we may contribute to the

evolution of optical microscopy and open-up the new way of achieving the optical images of high resolution, better than that can be reached through the conventional optics.

Chapter 2: Light coupling into surface plasmons

2.1 INTRODUCTION

In this chapter, we investigate the coupling mechanisms that efficiently translate the incident light into surface plasmons with specific aims on better controls of photons. First, unidirectional surface plasmon polarition (SPP) generation technologies, recently reported in Ref. [23,24] being established on slit-based geometries, are reviewed, and further characterized in the near-field in simulations. These methods presented may be suitable for various plasmonic applications in which localized, enhanced surface optical energy is required to be tailored and we discuss the effectiveness of such coupling methods for NSOM probe designs.

2.2 SINGLE SLIT-BASED COUPLER FOR UNIDIRECTIONAL PLASMON GENERATION

The behavior of SPPs, which is in strict TM modes of operation, has been well-explained with the electromagnetic field theory and proven to support strong light-matter interactions due to their highly localized field distribution in transverse direction. Since such surface wave is highly sensitive to the field disturbance in the near-field, the method of manipulating propagating surface plasmons with metallic corrugations have drawn special interest while triggering intensive development of intriguing applications. With a special aims on the efficient use of excited photons, coupled light can be guided in desired direction by a proper choice of plasmonic geometry.

Fundamental theory related to such phenomenon is being based on the diffractive properties of surface wave, and it has been possible to direct the surface light in the desired direction and suppress in others. In this section, the plasmonic geometry of interest is slit-based unidirectional couplers which are perforated in the opaque metal

screen. We survey two unidirectional SPP generation techniques reported in Ref. 23 and 24, and then further prove in the next section that efficient SPP generation can be integrated with the probe designs to realize subwavelength-sized light source with enhanced optical throughput. Detailed probe designs integrated with efficient SPP couplers for the near-field enhancement and focusing are presented in Chapter 3.

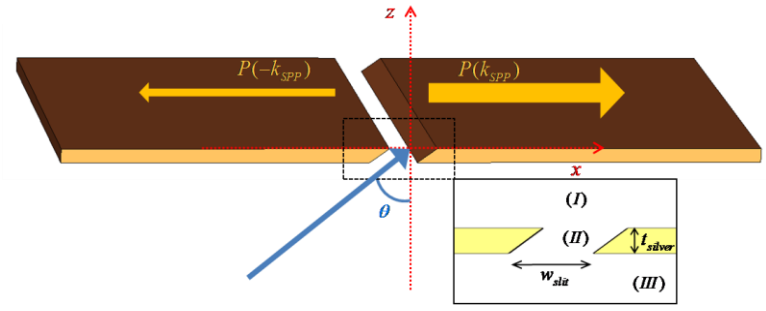

Figure 2-1. Conceptual schematic drawing of metal slit for unidirectional SPP generation. TM polarized plane wave is incident on backside; blue arrow denotes the wave vector of incident wave with incident angle. Tilting angle of slit and incident angle are identical in value $\theta = 54.7°$, and they are determined by the pyramidal probe geometry which may be fabricated by silicon-based bulk micromachinings. Note that w_{slit} and t_{slit} are the slit width and thickness of metal film, respectively.

The first coupler geometry is a single-slit coupler that the slit width is manipulated to generate unidirectionally propagating SPPs. SPP generation mechanisms of width-manipulated slit with oblique impinging waves is described with the guidance mode of slit and vectorial modal propagation at slit opening. To describe the out-coupled SPPs, slit diffraction is derived through the Maxwell's equation by applying proper boundary conditions.

A monochromatic wave $U(x,z,t) = u(x,z)e^{j\omega t}$ that can exist in the geometry can be represented as a two dimensional Fourier integral with respect to x and z [23,24]

directions, combined with the time evolution factor $e^{j\omega t}$. Note that the wave factor $u(x,z)$ indicates the magnetic field distribution of the TM wave existing in Figure 2-1. Angular spectrum of the slit geometry can be represented as in Equation 2.1; and the geometric parameters which maximize the value of $A\left(k_{spp:x}, z = t_{slit}\right)$ will be the optimized parameters for efficient SPP generation. $k_{spp:x}$ indicates the wave number of the SPP generated on metal/dielectric boundary [1], defined as $k_{spp} = k_o\sqrt{\varepsilon_m\varepsilon_d / (\varepsilon_m + \varepsilon_d)}$; where ε_m and ε_d are relative dielectric constants of metal and dielectric medium, respectively.

$$A\left(k_\alpha, z\right) = \int_{-\infty}^{\infty} u\left(x, y, z\right)\prod(x,z)\exp\left[jk_\alpha x\right]dx, \tag{2.1}$$

where $\prod(x,z)$ is the mathematical description of the slit geometry.

By exploring the behavior of electromagnetic wave near the slit, it can be deduced that the wave coming out of the slit will be efficiently coupled into the unidirectional surface plasmons when the design parameters, i.e. a slit width, and thickness of metal film, are properly chosen. Investigation on optimal design parameters of slit geometry for unidirectional SPP generation has been performed through two dimensional numerical simulations. To numerically investigate the directivity of generated SPP, we define the SPP directivity factor D by computing coupled magnetic field intensity on both sides of slit.

$$D = \frac{\left|H_y^{\,left}\right|}{\left|H_y^{\,right}\right|}, \tag{2.2}$$

where $H_y^{\,right}$ the magnetic field in y direction is calculated at the right side of the slit; and $H_y^{\,left}$ is the magnetic field at the left side of the slit. 2D simulations are carried out

to characterize the directivity and intensity of SPP generated around slit. A slit mounted on the silver film is considered other than perfect slit in order to investigate the coupling efficiency of generated SPP. The operational frequency of He:Ne laser (633nm) is considered for backside illumination. Relative dielectric constant of silver at 633nm is $\varepsilon_{silver} = -19 + i0.53$ [21] and surrounding medium is an air ($\varepsilon_{air} = 1$). Intensities of magnetic fields at left/right side of geometry are calculated with various value of slit width and unidirectional characteristics of width-manipulated slit geometry is illustrated in Figure 2-2.

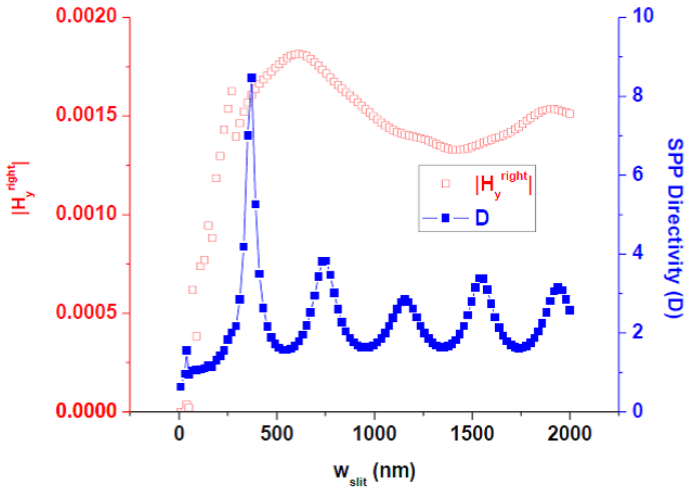

Figure 2-2. H field intensity and SPP directivity of slit geometry with various values of slit width w_{slit}. The magnetic field intensity on the left side (H_y^{left}) and right side (H_y^{right}) are calculated at the locations that are 2 μm away from the slit and 40 nm above the metal film.

From the 2D simulation results above we can choose the optimal design parameters that allow generating SPP with maximum directivity and relative high field intensity. Computed optimal slit width is 371 nm, and this value is well agreed with the slit width calculated from the cavity modal expansion presented in [23]. The thickness of

a metal film, 200 nm, is chosen to roughly match with Fabry-Pérot resonance condition [25]. It is interesting to notice that the metal slit geometry couples incident wave into SPPs in a bidirectional manner, D is close to 1, when the slit width is smaller than 170 nm, about a quarter wavelength of the incident wavelength. H field distribution of width-manipulated slit geometry with oblique illumination is described in Figure 2-3. With an optimized slit width, SPP directivity D exceeds 8, and the H field intensity is 7 times higher than that of 100 nm slit case.

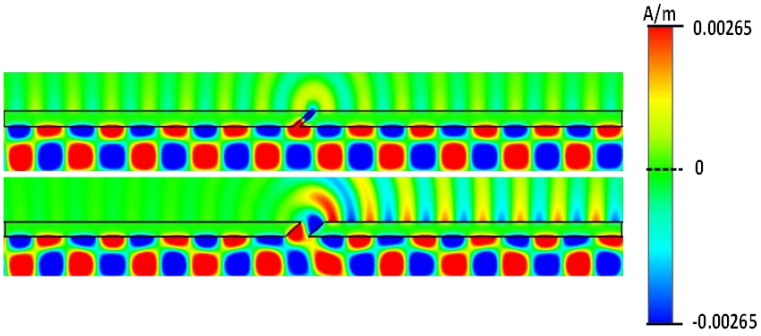

Figure 2-3. H_y field distribution around the slit geometry and near-field space with linear scale intensity. The slit geometries are simulated with the slit width of (a) 100 nm, and (b) 371 nm.

2.3 UNIDIRECTIONAL SURFACE PLASMON GENERATION BY REFLECTIVE GRATINGS

Unidirectional SPP can also be generated by the use of a proper grating geometry which provides destructive interference in one side of the slit geometry [24]. Diffraction condition sufficiently large grating geometry which can hold SPPs in resonance is satisfying the following condition.

$$k_{spp} = m\pi / p, \tag{2.3}$$

where p is the periodicity of grating corrugations, and m is the index of modal diffraction order of gratings.

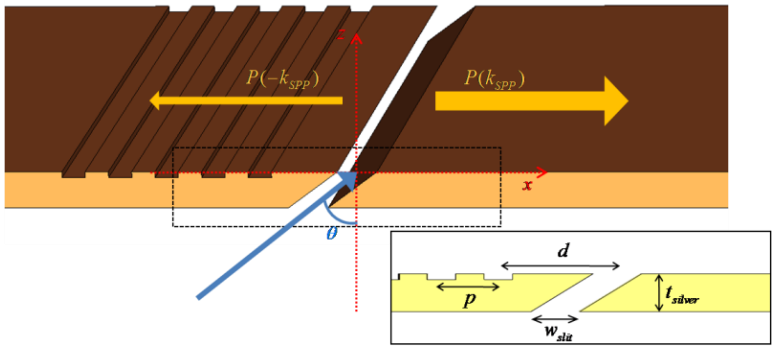

Figure 2-4. Schematic drawing of unidirectional surface plasmonic polariton(SPP) generation by tilted slit with a grating array. TM polarized plane wave is normally incident on backside; blue arrow denotes the wave vector of incident wave with incident angle $\theta = 54.7°$. Inset shows cross sectional schematic of the geometry. We note the geometrical design parameters: the periodicity of grating corrugations p, slit width w_{slit}, thickness of metal film t_{slit}, and the center to center distance between the slit and a first grating d.

Due to the presence of resonant grating array in Figure 2-4, standing wave which is in accordance with the wavelength of SPP is generated inside grooves. Thus, in turn, the groove geometry is now working as a SPP source generating SPP outward coherently. In order to achieve destructive interference on the left side of the slit, the reflective grating geometry may be placed with following rule

$$k_{spp} = n\pi / 2d, \tag{2.4}$$

where n is the index of diffraction order of positive integer. By following those simple diffraction conditions above, SPPs can be efficiently generated on the one side of slit geometry and suppressed on the other. Similar figure of merit defined in previous section

can be used to describe the performance of unidirectional SPP generation either. In order to verify the effect of presenting reflective gratings, 100 nm width slit geometry is considered for bidirectional SPP generation. Without presence of grating structure or disobeydance of condition in Equation 2.4, the efficiency of unidirectional SPP generation will be degraded.

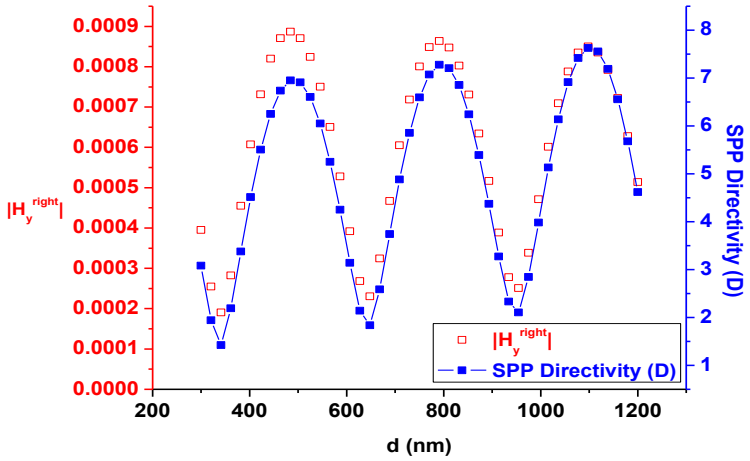

Figure 2-5. Unidirectional characteristics of two different slit geometries: (a) a single slit with optimized slit width and (b) a slit with an array of gratings. SPP directivity factor and magnetic field intensity at the right side versus various slit width. All fields, H_y^{left} and H_y^{right}, are calculated at the locations that are 2 μm away from the slit and 40 nm above the metal surface.

The H field intensity and directivity are investigated with various spacing d which defines a distance between slit and the beginning of periodic gratings. With constructive interference case where n is equal to even number, the unidirectional SPP generation is maximally suppressed; in contrast, with a destructive interference condition, where d is equal to 3 (or odd number), maximal directivity of around 8 can be achieved. H field distribution of two slit-based geometries having 100 nm slit with and

without reflective gratings, is presented in Figure 2-6, showing distinguishable directionality of coupled SPPS between them.

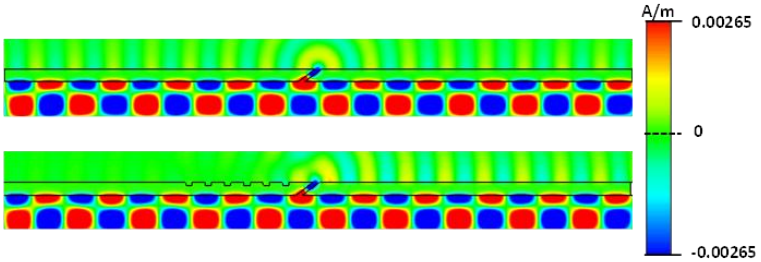

Figure 2-6. H_y field distribution around the slit geometry and near-field space with linear scale intensity. The 100 nm slit geometries are simulated (a) without and (b) with reflective gratings.

2.5 DISCUSSION AND CONCLUSION

Tailoring the movement of coupled waves has been a classical subject of interest in many research fields. Especially in the application at radio frequencies and microwaves, amplitude- and phase-manipulated arrays can couple and direct the incident wave in desired direction. Similar to the counterpart in the microwave engineering, slit-based coupler can translate the incident light into the surface plasmons propagating in a unidirectional manner. Following such knowledge, efficient SPP generation methods in Ref. 23 and 24 are reviewed and further investigated in simulations.

Presented coupling methods may appeal for the efficiency use of photons and be applied to the plasmonic probe designs while serving as a non-local light source that supply the optical power to the probe tip. In the next chapter, we discuss potential way to utilized presented slit-based couplers. Presented couplers are integrated with metal-coated probe tip and characterized in the near-field to evaluate their performance.

Chapter 3: Designs of efficient plasmonic scanning probe

3.1 INTRODUCTION

Near-field scanning microscopy (NSOM) is a versatile tool for investigating the sample surfaces, allowing the imaging of both optical signature and topographic information. By probing near-field interactions within the localized region of sample, high resolution optical images, which cannot be reached through the conventional optics, has been achieved with various probe designs. In particular, aperture-based NSOM probe [26.27] in the transmission-mode has shown promising results in terms of high-resolution imaging while guiding and focusing electromagnetic (EM) energy over the damping mode of waveguide of the small aperture. To obtain quality optical images in near-field, fundamental, physical requirements have to be satiated. First, the waveguide geometry of a probe including the aperture geometry needs to support the efficient transmission of optical energy; and second, a sharp tip dimension allowing access to the small region of interest is also necessary. By observing the near-field interaction which is coupled through the small aperture, one would achieve the high resolution of optical images better than 50 nm [26.27]. For the past decades, various aperture-based NSOM probe designs have been reported to satisfy such qualifications and break the diffraction limit of conventional optics, taking advantage of the local near-field [28-30]; however, the inherent low optical transmittance of NSOM probes associated with the small dimension of aperture for the high resolution imaging in general limits the performance of near-field scanning by impeding the signal discrimination over strong background noise signals.

To overcome such low optical transmission of aperture-based probe designs, the recent progress in NSOM probe design has been made utilizing the property of surface

plasmon wave [1,31], which is following the evanescent mode of propagation at metal and dielectric interface. In plasmonic nano-photonics, effective focusing and enhancing of near-field light within the small region of interest may rely on the configuration of metal geometry used [32-37]: the improved throughput with effective light confinement has been achieved by using the geometries for diffractive light focusing [32], build-up of aperture resonance [33,34], nano-antenna at aperture [35], and geometrical plasmon focusing [36,37]. Among the prominent progresses, one important probe design was devised [38] through the use of periodic corrugations perforated in metal film. One can further utilize the optical energy, coupled through an aperture, in more efficient way by focusing plasmonic surface waves before being dissipated by the propagation loss. A metallic probe with a tip aperture and concentric corrugations on its face could feature large field enhancement in the near-field of the tip apex [38]. Following the demonstration of such diffractive SPP focusing for NSOM applications, similar probe configurations have been studied in order to provide the enhanced signal to noise ratio (S/N) [39,40]. Although late studies on localized near-field enhancement of aperture-based probe design claim that the use of surface wave is being effective for the near-field focusing and enhancement, overall optical energy available for near-field scanning is sorely dependent on the limited optical energy coupled through the waveguide geometry of probe and small aperture. This allows the use of only fraction of impinging energy; thus, one may envision of the probe designs that can utilize the impinging light in more efficient way without suffering from the cut-off mode of waveguide and low transmittance of small aperture.

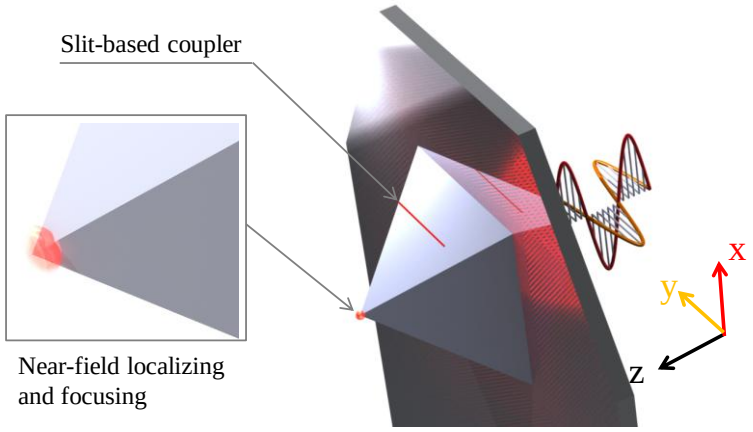

Figure 3-1. Probe geometry of interest, consisting of metallic probe tip and slit-based SPP coupler.

In this chapter, we present our recent theoretical study on novel plasmonic probe designs, providing the mechanism of efficient near-field focusing and localization [41]; and further extended study on plasmonic probe featuring wideband operation is also presented. The proposed probe configuration involves the designed non-local Surface Plasmon Plariton (SPP) coupler (see Chapter 2) launching surface plasmon waves in unidirectional way, and metal-coated probe body featuring a sharp dimension of apertureless tip. Slit-based non-local coupler designs [43,23] are employed to efficiently translate the impinging light into the SPPs on prove faces, and metal-coated sharp pyramidal geometry are considered to geometrically guide the surface energy at small tip apex. Unlike the conventional aperture-based probe designs in which the aperture is located at the cut-off region of probe waveguide, the proposed probe configurations may utilize more optical energy before being dissipated by the modal rejection. Herein, the metal-coated pyramidal probes are presented with various SPP generation mechanisms, showing extremely large field enhancement and high optical resolution. The proposed probes are characterized in the near-field with the finite-integration-technique (FIT)

based software package, CST Microwave Studio. In addition to the numerical study on the near-field focusing and enhancement for NSOM applications, we discuss potential way to introduce the wide bandwidth of operation to the probe geometry with a non-local SPP coupler. By employing a proper design of SPP coupler, a plasmonic probe possibly provides desired spectral response of operation.

3.2 APERTURELESS PLASMONIC PROBE DESIGNS

3.2.1 Single slit-based SPP couplers for the near-field focusing and localizing

We consider metal-coated, pyramidal-shaped dielectric probe geometry for the light localization and concentration, which can realized within the current silicon-based MEMS technologies [18,42] and nano-fabrication technique such as the bulk micromachining and focused ion beam (FIB) etching. Proposed probe configuration consists of sharp metallic (silver) apertureless tip with a diameter of 100 nm and a slit-based non-local SPP coupler perforated in 250 nm thick Ag film on probe face. Unlike classical aperture-based probe (with local light source) in which the most incident light is being cut-off before reaching to the tip aperture, a probe with non-local SPP couplers can utilize the impinging optical energy in more efficient way without suffering cut-off of waveguide mode. Upon the utilization of non-local coupler, launched SPPs can be guided toward tip side and focused by sharp probe geometry, enabling highly localized near-field enhancement at tip apex. To translate incident light to SPP in more efficient way, two different SPP generation mechanisms [43,23] are employed and integrated with probe geometry. Single slit supporting non-fundamental mode of waveguiding inside is mounted to realize type A probe, unidirectionally generating SPPs with an oblique incident of light. Optimal design parameter, slit width of 371 nm [41], is chosen to realize

highly directive SPP generation at 633 nm with a given tilted illumination (tilting angle of 54.4°). In type B probe, a single slit (100 nm in width) operating with only fundamental mode is mounted and backed Bragg reflector to direct coupled SPPs in unidirectional manner. Similar to type A probe design, generated SPPs can be guided along the face to tip apex with sharp probe tip geometry. For both type A and type B probe, non-local couplers were placed 1000 nm distant from a tip apex along the probe face.

With a classical single aperture probe, both type A and type B probe are numerically characterized and compared in near-field of the tip. Radially polarized illumination operating at 633 nm is considered to maximally take advantage of four SPP couplers on probe faces and to provide the constructive interference of axially polarized electric field. The calculated electric field intensity and the electric energy density of each probe are presented in Figure 3-2. To evaluate the optical resolution of proposed probes, the full-width-at-half-maximum (FWHM) is defined by the distribution of the electric energy density near the probe tip. Both calculated field distribution and electric energy density are compared to that of a canonical single aperture probe at 20nm distance from the tip. Compared to the conventional single aperture probe, design A and design B probes features extremely large near-field enhancements by a factor of 2119 and 1023, respectively. Similarly, electrical energy density of type A is boosted more than 4×106 times, and which of type B is improved by 6 orders without compromising FWHM. The calculated FWHMs of the three probes are: 148.84 nm (canonical aperture probe), 138.02 nm (Type A) and 171.3 nm (Type B). Within 100 nm range of tip-sample distance, the calculated FWHMs of type A and B probes are contained under 200 nm, and both probes still hold huge energy density enhancement as shown in Figure 3-3.

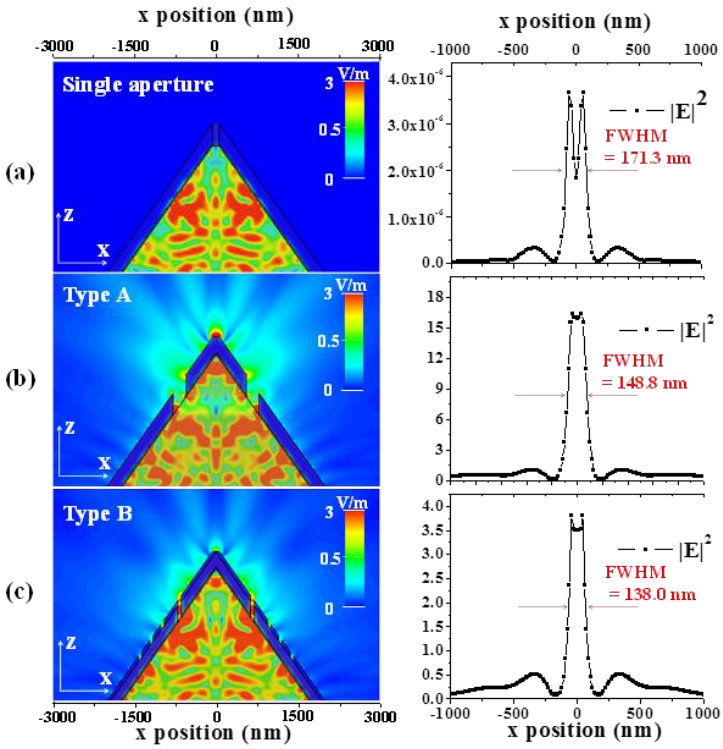

Figure 3-2. Calculated |E| field distributions of 3 different probes in x-z plane (left column) and |E|2 distribution along x axis with tip-sample distance of 20 nm (right column): (a) a classic single aperture probe with 100 nm-sized rectangular aperture, (b) type A probe, and (c) type B probe.

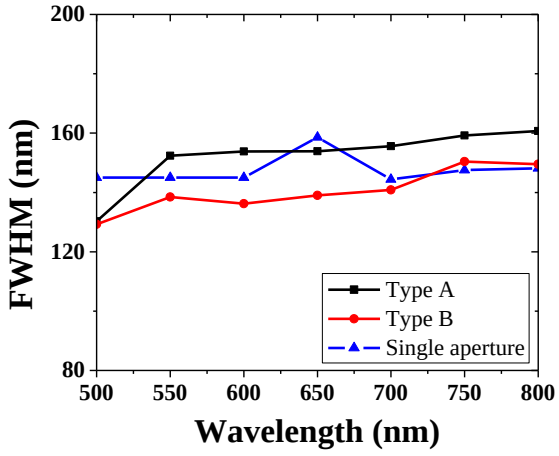

Figure 3-3. Spectral characteristic of three probes: type A, type B, and classical single aperture probe. FWHM along x-axis is calculated at tip-sample distance of 20 nm.

One important feature of proposed probe geometries is that the near-field optical resolution (FWHM) attainable in near-field is primary determined by physical dimension of tip apex as reported in previous study [45]. By reducing the tip size, one may obtain better optical resolution and improved near-field enhancement. Figure 3-4 shows the effect of tip size on the near-field enhancement and confinement especially for the type A probe. Type A with various tip diameters is characterized in near-field by the electric energy profiles, specifically FWHM at 20 nm tip-sample distance along x-direction, are calculated.

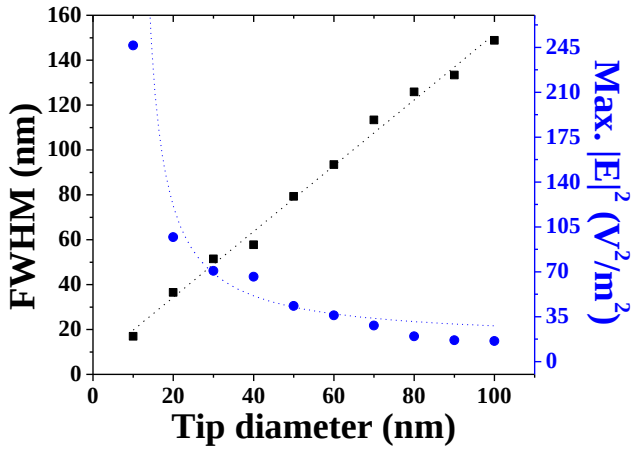

Figure 3-4. Computed near-field characteristics of type A probe with various tip diameters: optical resolutions (FWHMs) are calculated at tip-sample distance of 20 nm along x-direction (black squares) and the highest intensity of electric energy is calculated (blue circles). Note that dotted lines are fitting curves.

As presented the maximum value of near-field intensity is inversely proportional to the tip dimension while the defined optical resolution (i.e. FWHM) is in the opposite

proportionality. We note that such relationship between the tip size and near-field intensity is clearly distinctive from that of aperture-based probe, which is relying on the evanescent mode of transmission through small aperture showing extremely low transmission efficiency as the aperture size reduces. In this regard, the development of efficient NSOM probe may take advantage of our approach and becomes subject to realizing the sharp probe tip geometry with a proper design of efficient non-local SPP coupler.

3.2.2 Array of slits on apertureless probe for wideband operation

As discussed in the previous section, we have recognized that the near-field focusing and enhancement at probe tip can be achieved by efficient SPPs generation and proper design of near-field guiding geometry. This concept may be expanded to introduce the specific spectral functions for some applications. Since the spatial resolution of the proposed probe configuration counts on the geometrical sharpness of tip apex as shown in our previous study [41] and elsewhere [45], the proposed apertureless NSOM probe may feature various operating spectrum following that of the non-local coupler designed for specific purpose of interest. Among the desired spectral responses that can be achieved through the well-known coupler designs [46] at the radio frequency (RF), one may envision the wide bandwidth of operation for harvesting the various spectral signatures of specimen with a single probe. Since previously reported probe designs utilizing the diffractive focusing and near-field enhancement [38-40] are of the design for specific wavelength of operation, it would be impractical to observe wideband optical signatures with identical optical resolution. In contrast, the apertureless probe with wideband SPP coupler is being robust to the wavelength of operation (see Figure 3-3),

and may allow us to study the light-matter interaction at various wavelengths without degrading optical resolution. Studying absorption spectra of specimen in near-field, for instance, may broaden the scope of near-field optical microscopy by adopting the multi-color imaging of sample. In optic regime, the light-matter interaction varies with the change of operating frequency, so that one may achieve the hyper-spectral images of sample without having the target specimens stained with dyes.

To realize wideband operation, we may employ and modify a slit-based coupler design methodology which is frequently referred in the microwave engineering applications [46]. By manipulating the phase and intensity of wave out-coupled from each slit, one can tailor the overall spectral response of coupler. The proposed SPP coupler consists of an array of subwavelength-sized slits, each of which supporting only fundamental mode of waveguide inside; the array is designed following the rearranged series of Chebyshev polynomials to take advantage of fabrication convenience and to serve the wide bandwidth of operation. The transfer function S arranged from Chebyshev polynomials (Tn(secζ•cosψ)) of first kind for an array of N slits is derived and given as

$$S = \begin{cases} \sum_{i=0}^{(N-1)/2} T_{2i}\left(\sec\zeta\cos\psi\right) & \text{for } N = \text{odd number} \\ \sum_{i=1}^{N/2} T_{2i-1}\left(\sec\zeta\cos\psi\right) & \text{for } N = \text{even number} \end{cases}, \qquad (3.1)$$

where ζ is the edge of pass band over and phase span of ψ.

We note that the presented coupler design is being based on the summation of the Chebyshev responses of equal amplitude. Unlike the general, single Chebysheve response, the expected overall response S would not be equal-ripple spectra. Under given geometry inside probe where the incident waves obliquely impinge on the slit array, the

operating bandwidth can be controlled by the separation distance between each slit. We integrate the slit-based wideband SPP coupler to probe geometry and observe the near-field characteristics of probe.

To put the future experimental demonstration towards being more practical in terms of a simple optical setup configuration, it may be beneficiary to demonstrate the performance probe operating under the illumination of linearly polarized lights. In contrast to the case in which the radially polarized light is being used, the alignment of optics may not be required, and the coherent plane wave may be used to excite the probe. To theoretically demonstrate, the probe having a coupler on its single face is designed, and characterized in near-field under the illumination of linearly polarized plane light operating at 633 nm. In this probe configuration, the coupler integrated on the face of probe launches SPPs in unidirectional way over the wide bandwidth of operation, and the sharp probe geometry guides SPPs focus at tip apex (radius of 40 nm). The calculated electric field intensity and electric energy density of the probe with wideband SPP coupler in near-field are presented in Figure 3-5(b), comparing with the probe where a single slit coupler is used (Figure 3-5(a)). The wideband SPP coupler consists of 5 identical slits with the width of 50 nm and separation of 100 nm, and the first slit of the array is located 1500 nm away from the tip apex. In the case in which the single-slit coupler is being used, the SPPs are launched in bi-directional manner due to the existing fundamental mode supported only by such small slit. The passband spectra of the probe with wideband coupler is compared with that with a single slit coupler and presented in Figure 3-6.

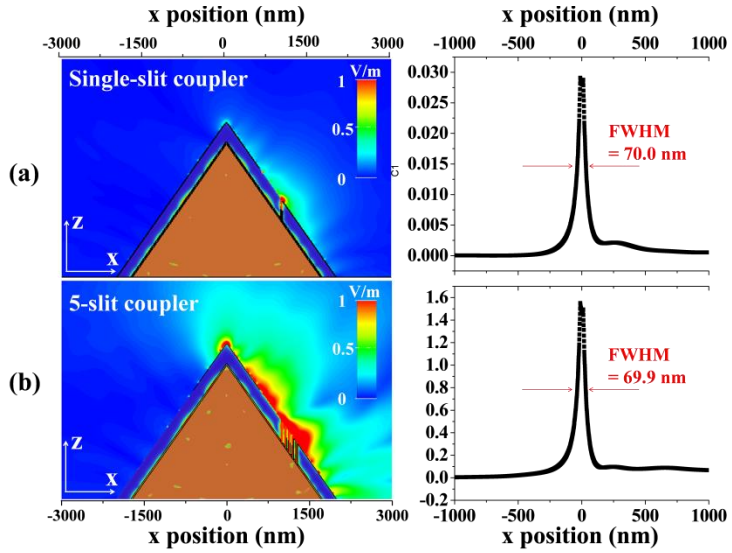

Figure 3-5. Calculated |E| field distributions of 2 different probes in x-z plane (left column) and |E|2 distribution along x axis with tip-sample distance of 20 nm (right column): (a) apertureless probe with 5-slit array, and (b) single slit coupler.

Numerical study in Figure 3-5 shows that the probe integrated with 5-slit coupler (Figure 3-5(b)) can guide and focus the near-field light within the very limited volume of interest (tip apex) in more efficient way. In comparison to the performance of probe with single-slit coupler, that with 5-slit coupler features higher near-field enhancement (7 times higher in terms of near-field intensity) by the efficient generation of SPPs and geometrical nano-focusing while containing the optical resolution (i.e. FWHM) of around 70 nm. We note that the calculated values of optical resolution of both probes are identical, and it proves that the geometry-dependent optical resolution is still held for the case that the linearly polarized light is used similar to the early statement in the previous section.

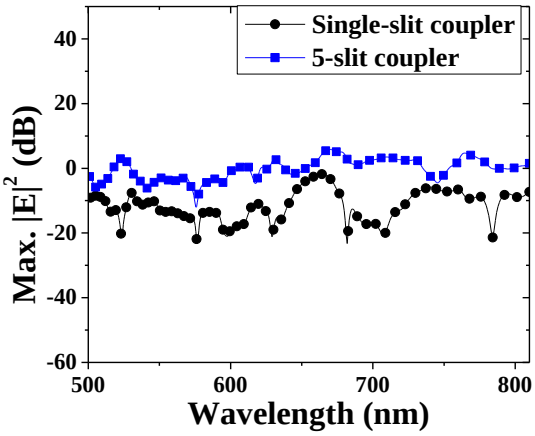

Figure 3-6. Maximum values of |E|2 of two probes calculated over the spectral range of interest. |E|2 is calculated at tip-sample distance of 20 nm and scaled in decibel. Note that the calculated spectrum is normalized to the intensity of impinging light (0 dB).

The spectral response of proposed probe geometry in near-field is characterized as well by observing the maximum value of electric energy density at tip-sample distance of 20 nm (see Figure 3-6). Two different probes have been numerically investigated and compared to each other: apertureless probe with a wide-band SPP coupler, and that with a single slit coupler. Numerical study in Figure 3-6 shows that the near-field enhancement can be achieved within the wide bandwidth of operation by adopting the slit array. In comparison to the probe with single-slit coupler, the probe with 5-slit array shows 11.05 dB higher electric energy density on average (with 1.23 dB less standard deviation) over the spectrum ranging from 500 nm to 810 nm.

3.3 Discussion and Conclusion

The property of surface plasmons at the metal and dielectric interface offers an intriguing way to focusing and localizing light within sub-wavelength scale volume.

Herein, we summarize the key findings from an intensive numerical study on the designs of plasmonic scanning probe. Proposed designs can provide extremely large near-field enhancement while containing electromagnetic energy in small volume, while offering the geometry-dependent spatial resolution. It is also discussed that desired spectral function, specifically wideband operation, maybe introduced to the NSOM probe by choosing a proper design methodology of non-local SPP coupler. Throughout manipulating the configuration of slit-based SPP coupler, a scanning probe appealing for wideband operation may be obtained. We believe that our probe designs can be realized within the scope of standard micro-/nano-fabrication technologies that reported elsewhere [18,42], while opening a new generation of the near-field scanning optical microscopy that serves the high optical-resolution imaging within tunable spectrum.

Chapter 4: Future plan

In this thesis, we have focused on the numerical study of efficient plasmonic probe designs which can break the diffraction limit and provide high optical throughput never being carried out by the conventional NSOM probe configuration. We theoretically demonstrate that efficient SPP generation can be applied to the design of plasmonic probe and used for the near-field focusing and enhancement. Specifically, coupler designs are reviewed and further investigated in the Chapter 2, and those applied to the probe design and proven being the effective methods of light coupling for the near-field focusing. Along with the theoretical investigations on the efficient use of photons for near-field scanning optical microscopy, the proposed plasmonic probes are fabricated by employing silicon-based micromachining and photoplastic casting method. Through the use of nanofabrication technology, we may realize the desired probe showing high fabrication throughput and having the physical dimension of tip apex less than 50 nm. Theoretically we have found that desired near-field focusing and enhancement can be achieved by geometrical nano-focusing and spectral response can be tailored by proper choice of coupler designs.

The ultimate goal of this project involves the development of NSOM system which can adopt and utilize the designed probes that are presented in this thesis. Upon the complete of NSOM system development, we will experimentally demonstrate new class of NSOM that feature high optical throughput and high optical resolution at the same time.

References

[1] H. Raether, Surface plasmons on smooth and rough surfaces and on gratings, (Springer-Verlag, Berlin, 1988).

[2] A. G. Curto, G. Volpe, T. H. Taminiau, M. P. Kreuzer, R. Quidant, and N. F. van Hulst, "Unidirectional emission of a quantum dot coupled to a Nanoantenna," Science **329**, 930-933 (2010).

[3] T. Hanke,G. Krauss,D. Träutlein,B. Wild,R. Bratschitsch, and A. Leitenstorfer, "Efficient nonlinear light emission of single gold optical antennas driven by few-cycle near-infrared pulses," Phys. Rev. Lett. **103**, 257404 (2009).

[4] S. Kühn, U. Håkanson, L. Rogobete, and V. Sandoghdar, "Enhancement of single-molecule fluorescence using a gold nanoparticle as an optical nanoantenna," Phys. Rev. Lett. **97**, 017402 (2006).

[5] A. V. Akimov, A. Mukherjee, C. L. Yu, D. E. Chang, A. S. Zibrov, P. R. Hemmer, H. Park, and M. D. Lukin, "Generation of single optical plasmons in metallic nanowires coupled to quantum dots," Nature **450**, 402-406 (2007).

[6] C. Ropers, C. C. Neacsu, T. Elsaesser, M. Albrecht, M. B. Raschke, and C. Lienau, "Grating-coupling of surface plasmons onto metallic tips: A nanoconfined light source," Nano Lett. **7**, 2784-2788 (2007).

[7] N. Chiu, C. Lin, J. Lee, C. Kuan, K. Wu, and C. Lee, "Enhanced luminescence of organic/metal nanostructure or grating coupler active long-range surface plasmonic device," Appl. Phys. Lett.**91**, 083114 (2007).

[8] Y. Wang, W. Srituravanich, C. Sun, and X. Zhang, "Plasmonic nearfield scanning probe with high transmission," Nano Lett. **8**, 3041-3045 (2008).

[9] N. Behr and M. B. Raschke, "Optical antenna properties of scanning probe tips: Plasmonic light scattering, tip−sample coupling, and near-field enhancement," J. Phys. Chem. C **112**, 3766-3773 (2008).

[10] G. Rui, W. Chen, and Q. Zhan, "High efficiency plasmonic probe design for parallel near-field optics applications," Opt. Express **19**, 5187-5195 (2011).

[11] E. M. Perassi, A. F. Scarpettini, M. E. Masip, A. V. Bragas, and E. A. Coronado, "Understanding the behavior of new plasmonic probes with sub-nanometric resolution in field enhanced scanning optical microscopy," J. Phys. Chem. C **115**, 10455–10461 (2011).

[12] M. Fleischer, C. Stanciu, F. Stade, J. Stadler, K. Braun, A. Heeren, M. Häffner, D. P. Kern, and A. J. Meixner, "Three-dimensional optical antennas: Nanocones in an apertureless scanning near-field microscope," Appl. Phys. Lett. **93**, 111114 (2008).

[13] P. Ginzburg and M. Orenstein, "Plasmonic transmission lines: from micro to nano scale with λ/4 impedance matching," Opt. Express **15**, 6762-6767 (2007).

[14] A. Alù and N. Engheta, "Optical nanotransmission lines: synthesis of planar left-handed metamaterials in the infrared and visible regimes," JOSA B **23**, 571-583 (2006).

[15] N. Engheta, A. Alu, and A. Salandrino, "Nanocircuit elements, nano-transmission lines and nano-antennas using plasmonic materials in the optical domain," IEEE Ant. Tech. 165-168 (2005).

[16] A. Alù and N. Engheta, "Three-dimensional nanotransmission lines at optical frequencies: A recipe for broadband negative-refraction optical metamaterials," Phys. Rev. B **75**, 024304 (2007).

[17] J. Rybczynski, K. Kempa, A. Herczynski, Y. Wang, M. J. Naughton, Z. F. Ren, Z. P. Huang, D. Cai, and M. Giersig, "Subwavelength waveguide for visible light," Appl. Phys. Lett. **90**, 021104 (2007).

[18] J. Lee, H. Shin, S. Kim, S. Hong, J. Chung, H. Park, and J. Moon, "Fabrication of atomic force microscope probe with low spring constant using SU-8 photoresist," Jpn. Appl. Phys. **42**, 1171-1174 (2003).

[19] G. Kim, B. Kim, M. Liebau, J. Huskens, D. N. Reinhoudt, and J. Brugger, "Surface modification with self-assembled monolayers for nanoscale replication of photoplastic MEMS," J. Microelectromech. S. **11**, 175-181 (2002).

[20] A. D. Rakic, A. B. Djurisic, J. M. Elazar, and M. L. Majewski, "Optical properties of metallic films for vertical-cavity optoelectronic devices," Appl. Opt. **37**, 5271–5283(1998).

[21] E. D. Palik and G. Ghosh, *Handbook of optical constants of solids*, E.D. Palik, 2 ed. (Academic, Orlando, Fla., 1985).

[22] Y. Xie, A. R. Zakharian, J. V. Moloney, and M. Mansuripur, "Transmission of light through slit apertures in metallic films," Opt. Express **12**, 6106-6121 (2004).

[23] H. Kim and B. Lee," Unidirectional surface plasmon polariton excitation on single slit with oblique backside illumination," Plasmonics **4**, 153-159 (2009).

[24] F. López-Tejeira, S. G. Rodrigo, L. Martín-Moreno, F. J. García-Vidal, E. Devaux, T. W. Ebbesen, J. R. Krenn, I. P. Radko, S. I. Bozhevolnyi, M. U. González, J. C. Weeber and A. Dereux, "Efficient unidirectional nanoslit couplers for surface plasmons," Nature Phys. **3**, 324 - 328 (2007).

[25] S. Astileana, Ph. Lalanneb and M. Palamarua, "Light transmission through metallic channels much smaller than the wavelength," Optics Comm. 175, 265-273 (2000).

[26] D. W. Pohl, W. Denk, and M. Lanz, "Optical stethoscopy: Image recording with resolution $\lambda/20$," Appl. Phys. Lett. **44**, 651 (1984).

[27] U. Dürig, DW Pohl, and F. Rohner, "Near-field optical-scanning microscopy," J. Appl. Phys. Lett. **59**, 3318 (1986).

[28] A. Harootunian, E. Betzig, M. Isaacson, and A. Lewis, "Super-resolution fluorescence near-field scanning optical microscopy ," Appl. Phys. Lett. **49**, 674-676 (1986).

[29] E. Betzig, M. Isaacson, and A. Lewis, "Collection mode near-field scanning optical microscopy," Appl. Phys. Lett. **51**, 2088 (1987).

[30] E. Betzig and J. K. Trautman, "Near-field optics: microscopy, spectroscopy, and surface modification beyond the diffraction limit," Science **257**, 189-195 (1992).

[31] J. A. Schuller, E. S. Barnard, W. Cai, Y. C. Jun, J. S. White, and M. L. Brongersma, "Plasmonics for extreme light concentration and manipulation," Nature Mater. **9**, 193-204 (2010).

[32] H. J. Lezec, A. Degiron, E. Devaux, R. A. Linke, L. Martin-Moreno, F. J. Garcia-Vidal, and T. W. Ebbesen, "Beaming light from a subwavelength aperture," Science **297**, 820-822 (2002).

[33] X. Shi and L. Hesselink, "Mechanisms for enhancing power throughput from planar nano-apertures for near-field optical data storage," Jpn. J. Appl. Phys. **41**, 1632-1635 (2002).

[34] N. M. DuBay, L. Wang, E. C. Kinzel, S. M. V. Uppuluri, and X. Xu, "Nanopatterning using NSOM probes integrated with high transmission nanoscale bowtie aperture," Opt. Express **16**, 2584-2589 (2008).

[35] T. H. Taminiau, R. J. Moerland, F. B. Segerink, L. Kuipers, and N. F. Van Hulst, "$\lambda/4$ resonance of an optical monopole antenna probed by single molecule fluorescence," Nano Lett. **7**, 28-33 (2007).

[36] C. Ropers, C. C. Neacsu, T. Elsaesser, M. Albrecht, M. B. Raschke, and C. Lienau, "Grating-coupling of surface plasmons onto metallic tips: A nanoconfined light source," Nano Lett. **7**, 2784–2788 (2009).

[37] C. C. Neacsu, S. Berweger, R. L. Olmon, L. V. Saraf, C. Ropers, and M. B. Raschke, "Near-field localization in plasmonic superfocusing: A nanoemitter on a tip," Nano Lett. **10**, 592-596 (2010).

[38] Y. Wang, W. Srituravanich, C. S. and X. Zhang, "Plasmonic nearfield scanning probe with high transmission," Nano Lett. **8**, 3041-3045 (2008).

[39] Y. Wang, Y. Huang, and X. J. Zhang, "Nanograting tip design for high power throughput near-field scanning aperture probe," Opt. Express **18**, 14004-14011 (2010).

[40] D. W. Kim, Y. C. Kim, O. Suwal, V. Jha, M. J. Park, and S. S. Choi, "Optimization of light-surface plasmon coupling by periodicity regulation for a pyramidal probe," Mat. Sci. Eng. B **149**, 242-246 (2008).

[41] Y. Lee, A. Alu, and X. J. Zhang, "Efficient apertureless scanning probes using patterned plasmonic surfaces," Opt. Express **19**, 25990-25999 (2011).

[42]. G. M. Kim, B. J. Kim, E.S. Ten Have, F. Segerink, N. F. Van Hulst, and J. Brugger, J. Micros. **209** (2003) 267-271.

[43]. F. López-Tejeira, Sergio G. Rodrigo1, L. Martín-Moreno, F. J. García-Vidal, E. Devaux, T. W. Ebbesen, J. R. Krenn, I. P. Radko, S. I. Bozhevolnyi, M. U. González, J. C. Weeber, and A. Dereux, Nature Phys. **3** (2007) 324-328.

[44]. H. Kim and B. Lee, "Unidirectional surface plasmon polariton excitation on single slit with oblique backside illumination," Plasmonics **4**, 153-159 (2009).

[45] M. Stockman, "Nanofocusing of optical energy in tapered plasmonic waveguides," Phys. Rev. Lett., **93**, 137404 (2004).

[46] D. M. Pozar, *Microwave Engineering*, Addison Wesley, 1990.

[47] D. Sander, R. Hoffman, V. Relling, and J. Muller, “Fabrication of metallic microstructures by electroplating using deep-etched silicon molds,” J. Microelectroch. Sys. **4**, 81-86 (1995).